



Effect of ceria on the structure and catalytic activity of V_2O_5/TiO_2-ZrO_2 for oxidehydrogenation of ethylbenzene to styrene utilizing CO_2 as soft oxidant

Komateedi N. Rao ^{a,b}, Benjaram M. Reddy ^a, B. Abhishek ^b, Yeong-Hui Seo ^b,
Nanzhe Jiang ^b, Sang-Eon Park ^{b,*}

^a Inorganic and Physical Chemistry Division, Indian Institute of Chemical Technology, Hyderabad 500 607, India

^b Laboratory of Nano-Green Catalysis, Department of Chemistry, Inha University, 253 Yonghyun-dong, Incheon 402-751, Republic of Korea

ARTICLE INFO

Article history:

Received 8 May 2009
Received in revised form 6 July 2009
Accepted 8 July 2009
Available online 15 July 2009

Keywords:

Oxidative dehydrogenation
Ethylbenzene
Carbon dioxide
 V_2O_5/TiO_2-ZrO_2
Styrene

ABSTRACT

The present study was undertaken to investigate the influence of ceria on the physicochemical and catalytic properties of V_2O_5/TiO_2-ZrO_2 for oxidative dehydrogenation of ethylbenzene to styrene utilizing CO_2 as a soft oxidant. Monolayer equivalents of ceria, vanadia and ceria–vanadia combination over TiO_2-ZrO_2 (TZ) support were impregnated by a coprecipitation and wet impregnation methods. Synthesized catalysts were characterized by using X-ray diffraction, Raman spectroscopy, X-ray photoelectron spectroscopy, temperature programmed reduction, transmission electron microscopy and BET surface area methods. The XRD profiles of 550 °C calcined samples revealed amorphous nature of the materials. Upon increasing calcination temperature to 750 °C, in addition to $ZrTiO_4$ peaks, few other lines due to ZrV_2O_7 and $CeVO_4$ were observed. The XPS V 2p results revealed the existence of V^{4+} and V^{5+} species at 550 and 750 °C calcinations temperatures, respectively. TEM analysis suggested the presence of nanosized (<7 nm) particles with narrow range distribution. Raman measurements confirmed the formation $ZrTiO_4$ under high temperature treatments. TPR measurements suggested a facile reduction of $CeO_2-V_2O_5/TZ$ sample. Among various samples evaluated, the $CeO_2-V_2O_5/TZ$ sample exhibited highest conversion and nearly 100% product selectivity. In particular, the addition of ceria to V_2O_5/TZ suppressed the coke deposition and allowed a stable and high catalytic activity.

© 2009 Elsevier B.V. All rights reserved.

1. Introduction

As industrial demand for styrene grows, its production via dehydrogenation (DH) of ethylbenzene (EB) is receiving greater importance. DH of styrene is highly endothermic reaction and requires high reaction temperatures (around 600–700 °C) and low ethylbenzene pressures [1–3]. Presently, more than 90% of styrene is produced based on catalytic dehydrogenation of EB. As a consequence of high reaction temperature and excess superheated steam, the conventional process suffers from poor economy and rapid catalyst deactivation owing to coke formation. Since the process is equilibrium-limited and energy intensive, there is a great interest for the development of an alternative methodology. Recently, oxidative dehydrogenation (ODH) process has been realized as one of the most elegant routes to produce styrene. Moreover, the ODH process has been widely investigated by variety of oxidizing agents such as dry air, O_2 , N_2O , SO_2 and so on [4–6]. It has been realized very recently that CO_2 can act as a soft

oxidant as well as diluent [2]. There are a number of additional benefits for utilizing CO_2 unlike the other oxidants. In particular, (i) there is no loss of latent heat for CO_2 because CO_2 stays in the gaseous form throughout the reaction [7]. (ii) CO_2 can decrease the partial pressure of reactants more effectively than steam and it has the highest heat capacity among various typical gases [8,9]. (iii) It also minimizes the significant quantities of valuable hydrocarbons leading to the generation of unwanted carbon oxides. (iv) Further, in the presence of CO_2 , coupling between reverse water–gas shift ($CO_2 + H_2 \leftrightarrow CO + H_2O$) and EBDH reaction becomes more favorable [9–11]. Therefore, utilization of CO_2 as a soft oxidant would be highly desirable for efficient conversion of EB to styrene.

Recently, several attempts were made in the literature for exploitation of ODH of EB by means of CO_2 as soft oxidant [9–20]. In this direction, a variety of active components like Fe-, Cr-, V-, Sn- and La-oxides [9–15] supported over different materials like carbonaceous materials, hydrotalcite-type compounds, zeolites, Al_2O_3 , Ga_2O_3 , ZrO_2 and TiO_2 [16–20] have been investigated. However, our recent studies revealed that titania–zirconia mixed oxides exhibit excellent catalytic activity and selectivity for the title reaction [12–14,20]. The significant features of TiO_2-ZrO_2 mixed oxides include a high specific surface area, profound acid–base and

* Corresponding author. Tel.: +82 32 860 7675; fax: +82 32 872 8670.

E-mail address: separk@inha.ac.kr (S.-E. Park).

redox properties together, high thermal stability and strong mechanical strength. In general, the ODH reaction using CO₂ as soft oxidant is believed to result in the formation of more carbonaceous deposits resulting in the fast deactivation of the catalysts. Therefore, there is an urge to design better catalyst systems, which can overcome the deactivation disadvantage. Recently, Murugan and Ramaswamy [21] reported a low temperature ODH of EB over ceria containing catalysts and noticed that ceria-based materials follow the Mars-van Krevelen mechanism and exhibit promising catalytic properties. Reddy and co-workers [22–26] also investigated the ceria-based materials for ODH and DH reactions, and uncovered that ceria containing materials suppress catalyst deactivation by preventing coke formation during the reaction. It is a known fact that CeO₂-based mixed oxides are effective catalysts for oxidation of different hydrocarbons and for the removal of total organic carbon from polluted waters from different sources. It has also been established that the presence of CeO₂ promotes various catalytic reactions such as CO₂ activation [27], CO oxidation [26,28] and CO/NO removal [29]. Therefore, ceria and ceria containing materials are receiving a great deal of attention due to the unique ability of ceria to shift easily between reduced and oxidized states (Ce³⁺ ↔ Ce⁴⁺) and to accommodate variable levels of bulk and surface oxygen vacancies [21–23,30]. These favorable characteristics make them as suitable for use as supports as well as catalysts in the processes wherein reaction conditions fluctuate between oxidizing and reducing environments. However, bulk cerium and vanadium oxides are susceptible to sintering leading to fall in the surface area and decrease in the stability of the structure during high-temperature applications. The rapid deactivation promotes the non-selective oxidations [31]. Hence, the combination of vanadia (known for its redox properties) and ceria (known for its oxygen storage and release functions) is expected to provide better catalytic systems.

In view of the problem of global warming and energy crisis, the utilization of CO₂ for a reaction like ODH of EB could be considered as a promising approach. Therefore, the present investigation was undertaken against the aforesaid background. In this study a CeO₂ promoted V₂O₅/TiO₂–ZrO₂ catalyst along with CeO₂/TiO₂–ZrO₂, V₂O₅/TiO₂–ZrO₂ and TiO₂–ZrO₂ were synthesized and evaluated for the ODH of EB using CO₂ as the soft oxidant. To determine the physicochemical properties of various samples synthesized, different characterization techniques namely, BET surface area (SA), pore size distribution (PSD), X-ray diffraction (XRD), Raman spectroscopy (RS), temperature programmed reduction (TPR) of H₂, transmission electron microscopy (TEM) and X-ray photoelectron spectroscopy (XPS) were employed. To know the deactivation phenomenon of catalysts, the spent catalysts were also subjected to XRD and XPS analysis.

2. Experimental

2.1. Catalyst preparation

The TiO₂–ZrO₂ (1:1 mole ratio) mixed oxide was synthesized by a coprecipitation method by hydrolysis with ammonium hydroxide. In a typical experiment, the required quantities of zirconyl(IV) nitrate hydrate (Acros Organics, USA) and titanium(IV) chloride (Yakuri Pure Chemicals, Japan) were dissolved separately in deionised water and mixed together. To this mixture solution, dilute aqueous ammonia was used as precipitating agent and the resultant precipitates were aged hydrothermally for 12 h at 100 °C [25,32]. The obtained precipitates were filtered off and washed several times with deionised water until free from anion impurities. The obtained cake was oven dried at 120 °C for 12 h and finally calcined at 550 °C for 6 h. On the calcined TiO₂–ZrO₂ (TZ) mixed oxide support, a monolayer equivalent of V₂O₅

(15 wt.%), CeO₂ (15 wt.%) and CeO₂–V₂O₅ (7.5 wt.% + 7.5 wt.%) were deposited by adopting a standard wet impregnation method. To carry out this, the desired quantities of ammonium metavanadate (Aldrich) and ceric ammonium nitrate (TCI, Japan) were dissolved in deionised water to which the finely powdered support was added with continuous stirring. The excess water was evaporated on a water-bath under vigorous stirring. The resulting material was once again oven dried at 120 °C for 12 h and subsequently calcined at 550 °C for 6 h in air atmosphere. Some portions of the finished samples were again heated at 750 °C for 6 h to investigate their thermal stability.

2.2. Catalyst characterization

Powder X-ray diffraction patterns were recorded on a Rigaku Multiflex instrument using nickel-filtered Cu K α (0.15418 nm) radiation source and a scintillation counter detector. The intensity data were collected over a 2θ range of 2–80° with a 0.02° step size and using a counting time of 1 s per point. Crystalline phases were identified by comparison with the reference data from International Center for Diffraction Data (ICDD) files. The BET surface area and BJH pore size distribution measurements were made by N₂ adsorption/desorption at liquid-nitrogen temperature using a Micromeritics ASAP 2020 instrument. Before analysis, samples were evacuated for 3–4 h at 250 °C in the degassing port of the instrument. Raman spectra were recorded on a LabRam HR800UV Raman spectrometer (Horiba Jobin-Yvon) equipped with a confocal microscope and liquid-nitrogen cooled CCD detector at ambient temperature and pressure. The emission line at 325 nm from He–Cd laser (Melles Griot Laser) was focused on the sample under microscope. The time of acquisition was adjusted according to the intensity of Raman scattering. The XPS measurements were made on a KRATOS (ESCA AXIS 165) spectrometer by using Mg K α (1253.6 eV) radiation as the excitation source. Charging of catalyst samples was corrected by setting the binding energy of adventitious carbon (C 1s) at 284.6 eV. The TEM images were obtained on a JEM-2010 (JEOL) instrument equipped with a slow-scan CCD camera and at an accelerating voltage of 400 kV. Samples were sonically dispersed in ethanol and deposited on a carbon coated copper grid before examination. The TPR measurements were made on a Pulse Chemisorb 2705 (Micromeritics, USA) instrument. Before the TPR measurement, the sample was preconditioned by passing dry air (20 ml/min) at 400 °C for 2 h and later the temperature was brought down to 100 °C. The TPR was run from 100 to 700 °C at a heating rate of 10 °C/min in 5% H₂ in argon gas mixture.

2.3. Catalyst activity

The catalytic activity for vapor phase ODH of EB was investigated in a down flow fixed-bed stainless steel microreactor. For each run, ~1.0 g of sample was loaded in the reactor. The reactor was heated to 600 °C at a rate of 2 °C/min in the flow of He (20 ml/min) and kept at this temperature for 2 h and He was replaced with CO₂ gas. The catalyst pretreatment was continued at 600 °C for 30 min with CO₂ (20 ml/min) before conducting the reaction. The EB was introduced into the preheating zone of the reactor through a liquid feed pump with a constant feed rate of 9.8 mmol/h. Gaseous and liquid products were analyzed simultaneously by an on-line gas chromatograph (Younlin Instrument, Acme 6000 Series, Korea) equipped with TCD and FID. For analysis of liquid products, HP-innowax column (30 m long, 0.32 mm i.d. and 0.25 μm film thickness) was employed and for the gaseous products Porapak N 80/100 column (6 ft × 1/8 in.) was used. The main liquid products analyzed were styrene, benzene, toluene, benzaldehyde, and acetophenone; and the gaseous products were hydrogen, methane, carbon monoxide and carbon dioxide.

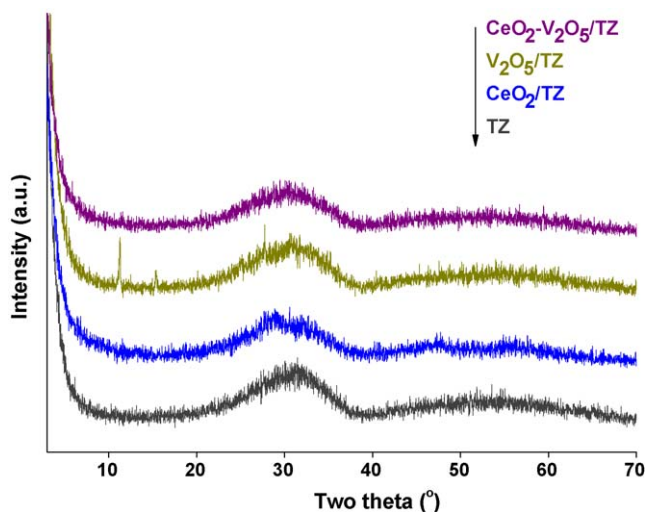


Fig. 1. X-ray powder diffractograms of $\text{TiO}_2\text{-}\text{ZrO}_2$ (TZ), $\text{CeO}_2\text{/TiO}_2\text{-}\text{ZrO}_2$, $\text{V}_2\text{O}_5\text{/TiO}_2\text{-}\text{ZrO}_2$, and $\text{CeO}_2\text{-}\text{V}_2\text{O}_5\text{/TiO}_2\text{-}\text{ZrO}_2$ samples calcined at 550°C .

3. Result and discussion

3.1. XRD and XPS

The powder XRD profiles of various samples calcined at 550°C are presented in Fig. 1. As can be noted from Fig. 1, no independent diffraction lines due to crystalline TiO_2 (anatase or rutile) and ZrO_2 (monoclinic, tetragonal or cubic) were observed. The X-ray diffraction profiles showed two broad peaks revealing the amorphous or poorly crystalline nature of catalysts. The XRD profiles of V_2O_5 and CeO_2 containing samples revealed that the impregnated oxides are in a highly dispersed form. The XRD profiles of promoted samples further suggest no substantial increase in the crystallinity of the support after impregnation with V_2O_5 and CeO_2 . However, in the present study the quantity of vanadia and ceria selected is lower than the theoretical monolayer capacity of the TZ support, based on its specific surface area [32]. To know the bulk composition of the impregnated materials and to understand their thermal stability at high temperatures, these samples were subjected to 750°C calcination and the corresponding XRD profiles are depicted in Fig. 2. All samples exhibited characteristic diffraction lines due to ZrTiO_4 compound [20,22–25]. In case of $\text{CeO}_2\text{/TZ}$ sample, there are no characteristic lines due to ceria indicating that cerium dioxide is in well dispersed state over the TZ support. Whereas V_2O_5 containing samples exhibited supplementary peaks pertaining to ZrV_2O_7 crystalline compound in addition to the ZrTiO_4 phase. In case of $\text{CeO}_2\text{-}\text{V}_2\text{O}_5\text{/TZ}$ sample, additional lines due to CeVO_4 are also noted. The crystallite size measurements were carried out by using the intense ZrTiO_4 line ($2\theta = 30^\circ$) of the 750°C calcined

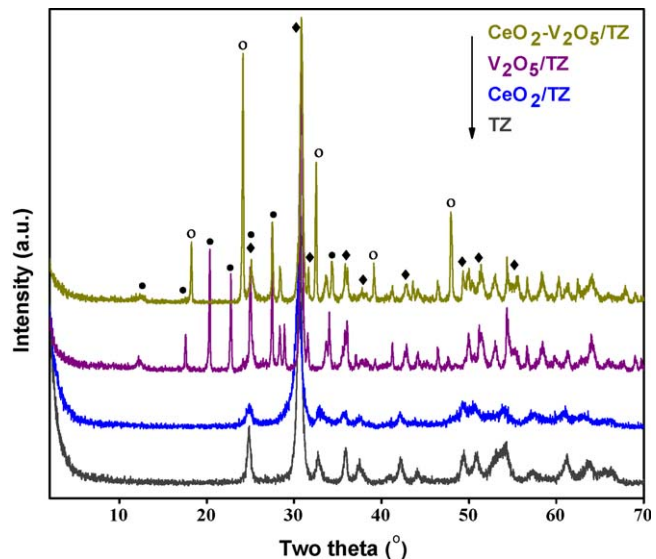


Fig. 2. X-ray powder diffractograms of $\text{TiO}_2\text{-}\text{ZrO}_2$ (TZ), $\text{CeO}_2\text{/TiO}_2\text{-}\text{ZrO}_2$, $\text{V}_2\text{O}_5\text{/TiO}_2\text{-}\text{ZrO}_2$, and $\text{CeO}_2\text{-}\text{V}_2\text{O}_5\text{/TiO}_2\text{-}\text{ZrO}_2$ samples calcined at 750°C : (◆) lines due to ZrTiO_4 ; (●) lines due to ZrV_2O_7 ; (○) lines due to CeVO_4 .

samples and observed that the addition of ceria to $\text{V}_2\text{O}_5\text{/TZ}$ decreases the crystallite size by ~ 5 nm. The pure support (TZ) and $\text{CeO}_2\text{/TZ}$ sample exhibited crystallite sizes of 17 and 12.7 nm, respectively. As revealed by XRD measurements (Figs. 1 and 2), the impregnated vanadia and ceria are in a highly dispersed state on the TZ support at 550°C . Upon increase of calcination temperature from 550 to 750°C , binary compounds such as ZrV_2O_7 and CeVO_4 in addition to ZrTiO_4 were observed.

To investigate the surface composition of various catalysts, XPS measurements were performed and the corresponding binding energy values of the elements O 1s, Ce 3d, Zr 3d, Ti 2p, and V 2p are listed in Table 1. The O 1s core level XPS profiles of various samples subjected to 550 and 750°C thermal treatments are shown in Fig. 3A and B, respectively. As can be observed from these figures, all the profiles consist of broad peaks ranging from 528 to 534 eV, which could be assigned to the lattice oxygen associated with the metal oxides [23,26]. The O 1s profiles are more complicated due to the overlapping contribution of oxygen from titania, zirconia, ceria, vanadia and from their mixed oxide compounds. With increase of calcination temperature a small increase in the binding energy values (Table 1) and sharpening of the peaks (Fig. 3B) are observed which could be due to better crystallization of the individual and/or mixed oxides inline with XRD analysis. Of course, it is well-known that the XPS peak intensity depends on both ion density and its chemical environment. The oxygen ion density in various samples is expected to be same. Therefore, the decrease in the peak

Table 1

BET surface area, pore volume and binding energy values of $\text{TiO}_2\text{-}\text{ZrO}_2$ (TZ), $\text{CeO}_2\text{/TiO}_2\text{-}\text{ZrO}_2$, $\text{V}_2\text{O}_5\text{/TiO}_2\text{-}\text{ZrO}_2$ and $\text{CeO}_2\text{-}\text{V}_2\text{O}_5\text{/TiO}_2\text{-}\text{ZrO}_2$ samples calcined at 550 and 750°C .

Sample	Surface area (m^2/g)	Pore volume (ml/g)	Binding energy (eV)				
			O 1s	Ce 3d _{5/2}	Zr 3d _{5/2}	Ti 2p _{3/2}	V 2p _{3/2}
Calcined at 550°C							
TZ	207	0.65	530.0	–	182.1	458.5	–
$\text{V}_2\text{O}_5\text{/TZ}$	175	0.46	530.0	–	182.0	458.5	516.3
$\text{CeO}_2\text{/TZ}$	189	0.51	529.9	882.4	182.0	458.4	–
$\text{CeO}_2\text{-}\text{V}_2\text{O}_5\text{/TZ}$	170	0.45	530.0	882.1	182.1	458.5	516.7
Calcined at 750°C							
TZ	112	–	530.5	–	182.7	459.1	–
$\text{V}_2\text{O}_5\text{/TZ}$	82	–	530.3	–	182.5	458.8	517.4
$\text{CeO}_2\text{/TZ}$	96	–	530.1	882.8	182.2	458.7	–
$\text{CeO}_2\text{-}\text{V}_2\text{O}_5\text{/TZ}$	88	–	530.2	883.2	182.4	458.9	517.4

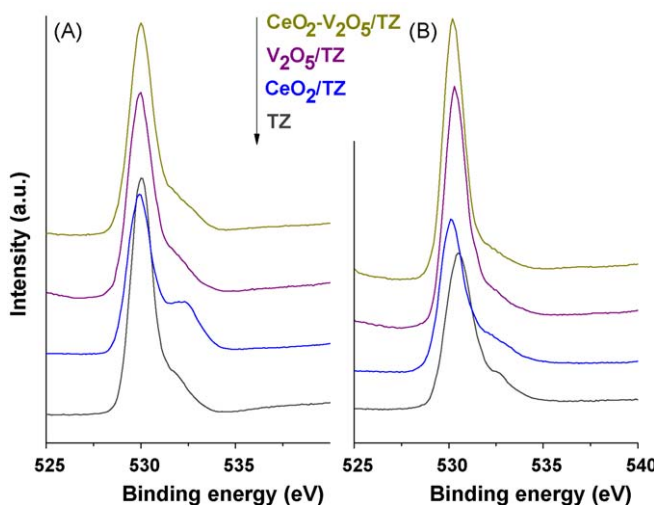


Fig. 3. O 1s XPS profile of TiO₂-ZrO₂ (TZ), CeO₂/TiO₂-ZrO₂, V₂O₅/TiO₂-ZrO₂, and CeO₂-V₂O₅/TiO₂-ZrO₂ samples calcined at 550 °C (A) and 750 °C (B).

intensity can be attributed to different chemical environments [23,32].

V 2p photoelectron peaks of the V₂O₅/TZ and CeO₂-V₂O₅/TZ catalysts calcined at 550 and 750 °C are shown in Fig. 4. The 550 °C calcined samples exhibited broad V 2p_{3/2} lines at ~516.3 eV; it is probably due to the presence of V⁴⁺ species over the surface. However, with increase of calcination temperature from 550 to 750 °C, the binding energy of V 2p_{3/2} increased from 516.3 to 517.4 eV (Table 1), an indication of increase in the oxidation state of vanadium that could be due to the formation of crystalline zirconium bivanadate. Vanadia in the 4+ oxidation state is stabilized on the amorphous TZ mixed oxide support when calcined at 550 °C [33]. As the calcination temperature increased, the formation of crystalline ZrTiO₄ and ZrV₂O₇ occurred, thereby decreasing the proportion of amorphous material. Thus, the newly formed crystalline ZrV₂O₇ compound stabilizes in the 5+ state of vanadium. From these data it is also clear that the binding energy of the V 2p_{3/2} peak is more sensitive to the nature of the carrier material [34,35]. The intensity of V 2p peak decreased with an increase in the calcination temperature for V₂O₅/TZ system,

whereas no such change was observed in the case of CeO₂-V₂O₅/TZ catalyst. This observation suggests the addition of ceria has stabilized the vanadia and suppressed the formation of specific compounds. The same observation was also illustrated from the XRD analysis. Table 1 discloses the core level electron binding energies of Zr 3d and Ti 2p for various samples calcined at two different temperatures. The photoelectron signals of Ti 2p are observed at 458.5 and 464.4 eV corresponding to the spin orbital multiplets of Ti 2p_{3/2} and Ti 2p_{1/2}, respectively [36]. Both Zr 3d and Ti 3d binding energies represent the presence of 4+ oxidation state for Zr and Ti. Interestingly, the binding energy values of Zr and Ti core levels increased with increase in the calcination temperature. This could be due to better crystallization of the materials and formation of new phases like ZrTiO₄ and ZrV₂O₇ [36]. Recently, Victor and Krupanidhi [37] also reported the O 1s, Zr 3d and Ti 2p BE values for ZrTiO₄ at 530.27, 182.24 and 458.66 eV, respectively which are close to the present XPS data. The present results are thus corroborating very well with the earlier findings.

The Ce 3d XPS profiles of CeO₂/TZ and CeO₂-V₂O₅/TZ samples calcined at 550 and 750 °C are shown in Fig. 5. As can be noted from the figure, the Ce 3d profiles are more complicated due to mixing of Ce 4f levels with O 2p states. The notation of the Ce 3d peaks in the present study are envisaged as elucidated in the literature [23,38]. Two sets of spin-orbit multiplets, corresponding to the 3d_{3/2} and 3d_{5/2} contributions are labeled as *u* and *v*, respectively. The *u'''/v''* doublet is due to the primary photoemission from Ce⁴⁺. The *u/v* and *u''/v''* doublets are shakedown features resulting from the transfer of one or two electrons from a filled O 2p orbital to an empty Ce 4f orbital. The *u₀*, *v₀* and *u'/v'* doublet are due to photoemission from Ce³⁺ cations. As previously pointed out, the XPS spectrum of CeO₂/TZ sample calcined at 550 °C exhibits peaks due to the presence of both Ce⁴⁺ and Ce³⁺, thus implying that cerium is present at the surface in both 4+ and 3+ oxidation states [23,26,33]. On high temperature calcination as well as addition of vanadia the binding energy values of Ce 3d shifted slightly to higher side, suggesting small shift in the binding energies that could be due to different metal ions environment near the cerium sites.

3.2. BET surface area and pore volume

The specific surface areas of various samples calcined at 550 and 750 °C are presented in Table 1. As can be noted from Table 1,

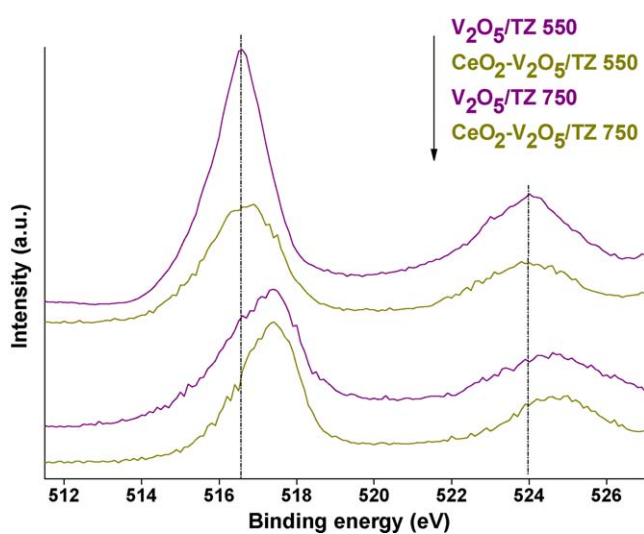


Fig. 4. V 2p core level XPS profile of V₂O₅/TiO₂-ZrO₂ and CeO₂-V₂O₅/TiO₂-ZrO₂ samples calcined at 550 °C.

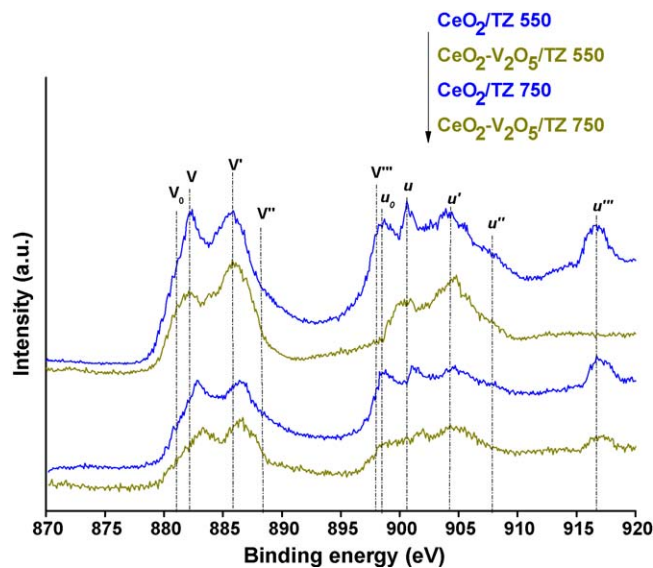


Fig. 5. Ce 3d XPS profile of CeO₂/TiO₂-ZrO₂ and CeO₂-V₂O₅/TiO₂-ZrO₂ samples calcined at 550 and 750 °C.

the synthesized TZ mixed oxide exhibited a high specific surface area of $207 \text{ m}^2/\text{g}$. Interestingly, it is higher than its individual component oxides, namely TiO_2 ($15 \text{ m}^2/\text{g}$) and ZrO_2 ($25 \text{ m}^2/\text{g}$) [13,14]. The high specific surface area of the titania–zirconia mixed oxide is due to the amorphous nature as well as the porosity of the material. The porosity of the synthesized materials is ascribed to the preparation method adopted and the precursors used in the present investigation. With increase in the calcination temperature there is a sudden drop in the surface area that could be attributed to the formation of nonporous TiZrO_4 . Of course, there is slight decrease in the surface area and pore volume in the case of vanadia and ceria impregnated samples (Table 1). The decrease in the specific surface area after impregnating with V_2O_5 or CeO_2 is due to various factors, mainly, penetration of the deposited active oxides into the pores of the support thereby narrowing its pore diameter and blocking some of the micropores, and solid-state reaction between the dispersed active oxide and the supporting material [23,26].

3.3. Raman spectroscopy and TEM

The existence of TiZrO_4 is further confirmed by Raman spectra as shown in Fig. 6. The spectrum of TZ sample calcined at 550°C mainly contained broad bands ranging from 200 to 370 cm^{-1} , 420 to 475 cm^{-1} and 680 to 890 cm^{-1} , which should be assigned as an amorphous material [37,39]. Thermal treatment of TZ in air atmosphere at 750°C leads to drastic changes in the Raman spectrum. The position and shape of these bands are different from either TiO_2 or ZrO_2 . As reported in the literature, the classification of each active mode of titania–zirconia mixed oxide by Raman spectrum is very difficult due to the structural conformation of this oxide [40]. However, a comparison with literature results of the number and position of peaks of the Raman spectra (Fig. 6) show a minimal discrepancy. Some of the fluctuations are related to different syntheses methodologies, in particular due to the difference in the heat treatments [39,40]. The spectrum exhibited

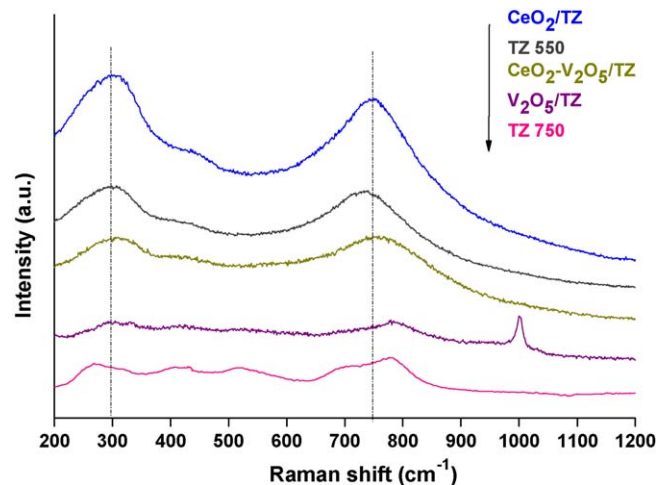


Fig. 6. Raman spectra of $\text{TiO}_2\text{--ZrO}_2$ (TZ 550), $\text{CeO}_2\text{/TiO}_2\text{--ZrO}_2$, $\text{V}_2\text{O}_5\text{/TiO}_2\text{--ZrO}_2$, and $\text{CeO}_2\text{-V}_2\text{O}_5\text{/TiO}_2\text{--ZrO}_2$ samples calcined at 550°C and $\text{TiO}_2\text{--ZrO}_2$ (TZ 750) sample calcined at 750°C .

bands (263 , 337 , 478 , 635 , and 784 cm^{-1}) at low frequency range. Based on the above arguments, the observed bands could be assigned to the existence of TiZrO_4 composition. Thus Raman results indicate the presence of zirconia in titania with the formation of TiZrO_4 that retard the phase transformation and thereby improving the textual properties at high temperatures. The $\text{V}_2\text{O}_5\text{/TZ}$ sample exhibited mainly two broad bands in the high frequency region from 700 to 1100 cm^{-1} , centered at about 775 and 1002 cm^{-1} , and these bands can be assigned to the formation of ZrV_2O_7 compound. Present results are in well agreement with the previous reports on $\text{V}_2\text{O}_5\text{/ZrO}_2$ systems, where the formation of ZrV_2O_7 was observed at higher calcination temperatures [41]. In the case of $\text{V}_2\text{O}_5\text{/TZ}$ sample, in addition to the broad bands of ZrTiO_4 and ZrV_2O_7 , a few extra broad signals due to the dispersed

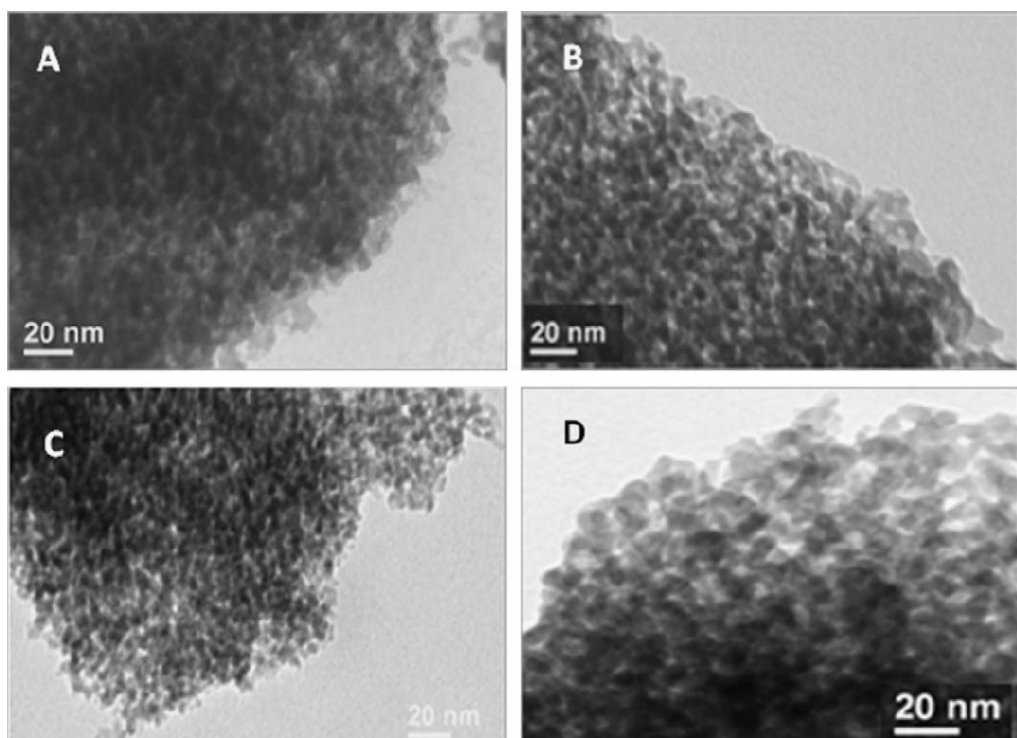


Fig. 7. TEM images of $\text{CeO}_2\text{-V}_2\text{O}_5\text{/TiO}_2\text{-ZrO}_2$ (A), $\text{V}_2\text{O}_5\text{/TiO}_2\text{-ZrO}_2$ (B), $\text{CeO}_2\text{/TiO}_2\text{-ZrO}_2$ (C) and $\text{TiO}_2\text{-ZrO}_2$ (D) samples calcined at 550°C .

vanadium oxide have been noted. In the case of CeO_2/TZ and $\text{CeO}_2\text{-V}_2\text{O}_5/\text{TZ}$ samples, only the broad background bands due to an amorphous ZrTiO_4 compound could be noted. Pure CeO_2 exhibits a band at 460 cm^{-1} and smaller bands at 239 and 590 cm^{-1} , respectively [42]. On the whole, the Raman measurements supported the observations made from XRD and XPS techniques.

To know the textural properties of various samples calcined at 550°C , TEM analysis was performed and the representative micrographs are presented in Fig. 7. As shown in Fig. 7, the TEM results are supporting the information obtained from other techniques. The $\text{TiO}_2\text{-ZrO}_2$ support is composed of snowflake type networks with nanometer-sized particles (Fig. 7D). This morphology generally leads to a loose structure with high specific surface area and pore volume, which has been confirmed by N_2 adsorption measurements. In all the images, small, well faceted particles with narrow range distribution were clearly visible. The impregnated active components (ceria and vanadia) seems to be well distributed on the support, i.e. homogeneous in nature. It is a known fact that control of microstructures is an important factor for the improvement of catalytic activity. Moreover, the addition of vanadium and cerium oxides had strong influence on the particle size of the $\text{TiO}_2\text{-ZrO}_2$ support as revealed by the TEM images. Further, TEM image of $\text{CeO}_2\text{-V}_2\text{O}_5/\text{TZ}$ sample revealed the combination features of CeO_2/TZ and $\text{V}_2\text{O}_5/\text{TZ}$ samples, respectively. In particular, the vanadium containing samples exhibited enhanced grain size compared to the other samples. As mentioned earlier, the accelerated particle size increase is due to better crystallization of TiO_2 and ZrO_2 , which are influenced by vanadium oxide [20,22].

3.4. Temperature programming reduction

To assess the reducibility of the dispersed compounds and interaction between support and the active components, temperature programming reduction was performed. The H_2 -TPR profiles of various samples calcined at 550°C are displayed in Fig. 8. TPR patterns revealed interesting information about the relative reducibility of the mixed oxides. The TZ support exhibited a sharp high temperature reduction peak at $\sim 748^\circ\text{C}$ and another broad peak at $\sim 870^\circ\text{C}$. This clearly shows that the TZ mixed oxide is quite stable due to the formation of an amorphous or poorly crystalline ZrTiO_4 compound [12–14,36]. There is a small combination negative peak observed at around 720°C which might be due to release of substrate by the support or from the formation of new phase as TPR temperature was higher than

the original calcination temperature [43]. In general, pure V_2O_5 is reduced by hydrogen in four characteristic steps [44]. According to Bosch et al. [44] the four steps of the reduction process of vanadia was described as $\text{V}_2\text{O}_5 \rightarrow \text{V}_6\text{O}_{13} \rightarrow \text{VO}_2 \rightarrow \text{V}_n\text{O}_{2n-1} \rightarrow \text{V}_2\text{O}_3$ ($4 < n < 8$). The reduction of pure V_2O_5 was observed only at temperatures above 700°C . However, the TPR profiles of the vanadia contained catalysts exhibited peaks at lower temperatures (Fig. 8) compared to the pure V_2O_5 . Moreover, the reduction temperatures of all the peaks were decreased due to the influence of the TZ support. Normally, the crystallite size combined with crystal orientation play a major role in the reduction behavior of various oxides. As envisaged in the literature, the unsupported V_2O_5 has a random orientation of various crystallographic planes exposed to the reduction gas mixture, whereas the supported V_2O_5 displays a preferred orientation and exhibits better reducibility. Accordingly, the dispersed vanadia over the TZ support is expected to reduce at lower temperatures than the bulk V_2O_5 . In the case of CeO_2 containing sample two low intense hydrogen consumption bands were observed at ~ 475 and 780°C due to the reduction of surface oxygen and bulk reduction of $\text{CeO}_2 \rightarrow \text{Ce}_2\text{O}_3$, respectively. Interestingly, the $\text{CeO}_2\text{-V}_2\text{O}_5/\text{TZ}$ sample exhibited a broad and well defined reduction peak at 598°C and another weak and broad peak at 780°C . This profile is different from the reduction profiles of $\text{V}_2\text{O}_5/\text{TZ}$ and CeO_2/TZ samples. The intense peak is primarily due to the reduction of the dispersed ceria–vanadia mixed oxide phase over the TZ support, which is formed owing to solid-state reactions between them. It can be noted that the addition of ceria to $\text{V}_2\text{O}_5/\text{TZ}$ sample promoted the reducibility as well as the dispersion of vanadium oxide species. The TPR peaks were not well resolved under the experimental conditions employed in the present study. Therefore, quantification of the data was not attempted.

3.5. Activity studies

The activity studies for oxidehydrogenation of EB were carried out in the vapor phase at normal atmospheric pressure employing CO_2 as a mild oxidant. Due to the endothermic nature of the reaction, for all the catalytic systems an increasing trend of EB conversion was observed with increasing reaction temperature. The promoted samples exhibited better activity compared to the parent TZ support. Our earlier study revealed that TZ mixed oxide exhibits exceptionally better conversion and product selectivity than its individual component oxides under identical reaction conditions [12–14]. The observed high activity and selectivity of the TZ was proved to be due to the formation of an amorphous compound, enhancement in the specific surface area, and an increase in the number and strength of acid–base sites. As reported in the literature, it has also been observed that initially with time-on-stream there is an enhancement in the activity due to the formation of a thin layer of carbonaceous deposits, which promote the ODH activity [45]. Hence, for better comparison the catalytic data obtained after 3–4 h has been considered. Among various samples evaluated, the $\text{CeO}_2\text{-V}_2\text{O}_5/\text{TZ}$ sample exhibited highest conversion (56%) and product selectivity (98%).

A fast catalyst deactivation is often encountered on most of the catalytic systems in the dehydrogenation of EB due to coke formation. Therefore, time-on-stream studies were performed to understand the behavior of catalysts. A series of time-on-stream studies were carried out at a constant temperature and optimum space velocity and accounted in Fig. 9. A fast deactivation of $\text{V}_2\text{O}_5/\text{TZ}$ sample was clearly seen from the figure and the faster deactivation is owing to heavy coke deposition over the surface of the catalyst as established by an increase in the weight of catalyst after the reaction [45]. Further, the activities of other catalysts (except $\text{V}_2\text{O}_5/\text{TZ}$) were found to improve with time in the first few hours of the reaction and there is no drastic fall in the activity

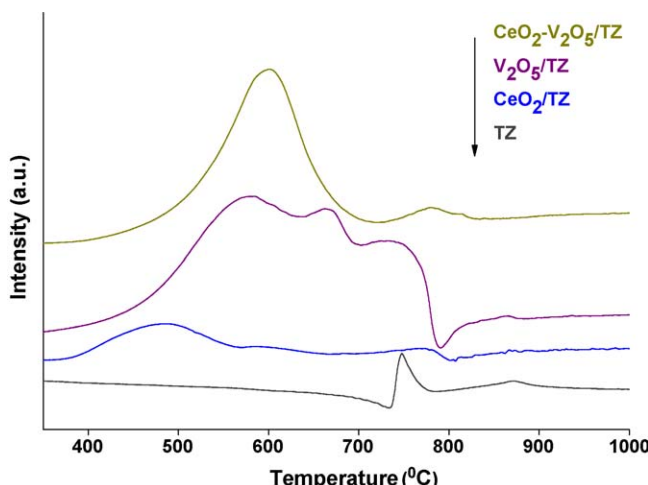


Fig. 8. The TPR (H_2) profiles of $\text{TiO}_2\text{-ZrO}_2$ (TZ), $\text{CeO}_2\text{/TiO}_2\text{-ZrO}_2$, $\text{V}_2\text{O}_5\text{/TiO}_2\text{-ZrO}_2$, and $\text{CeO}_2\text{-V}_2\text{O}_5\text{/TiO}_2\text{-ZrO}_2$ samples calcined at 550°C .

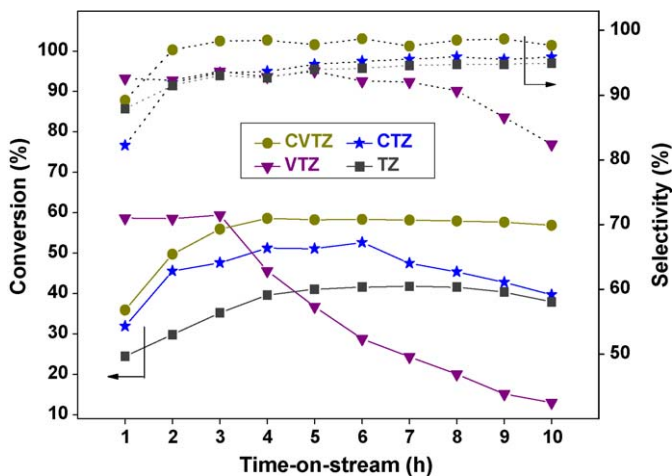


Fig. 9. Variation of catalytic activity and selectivity with time-on-stream over $\text{TiO}_2\text{-}\text{ZrO}_2$ (TZ), $\text{CeO}_2\text{/TiO}_2\text{-}\text{ZrO}_2$ (CTZ), $\text{V}_2\text{O}_5\text{/TiO}_2\text{-}\text{ZrO}_2$ (VTZ) and $\text{CeO}_2\text{-}\text{V}_2\text{O}_5\text{/TiO}_2\text{-}\text{ZrO}_2$ (CVTZ) samples. Reaction conditions: $T = 600^\circ\text{C}$, $P = 1$ atm, $\text{W/F} = 16.73$ g cat h/mol, $\text{CO}_2/\text{EB} = 5.1$ (molar ratio).

beyond 10 h of time-on-stream experiments. Interestingly, ceria-vanadia combination sample showed increased conversion in the first 4 h then remained constant up to 10 h with higher conversion and almost 100% selectivity. Therefore, the addition of ceria to vanadia improved the catalytic activity in terms of conversion and selectivity by preventing excess coke deposition over the catalyst surface. The stable activity of ceria-based catalysts is mainly due to facile oxygen transport from the bulk of CeO_2 [21,25]. The remarkable ability of CeO_2 in $\text{V}_2\text{O}_5\text{/TZ}$ catalysts to obtain a high and stable activity is clearly apparent from the present study. To gain information about the deactivation phenomenon of these catalysts, the spent catalysts (after time-on-stream) were subjected to XRD and XPS analysis.

Fig. 10 shows the X-ray powder diffraction profiles of used catalysts. As can be noted from the figure, except for $\text{V}_2\text{O}_5\text{/TZ}$ sample there no significant change in the XRD patterns of used and fresh (Fig. 1) samples. Hence, after the time-on-stream measurements also the crystallinity and bulk composition of the catalysts remained unaltered. Whereas, $\text{V}_2\text{O}_5\text{/TZ}$ sample showed lines due to the crystalline ZrTiO_4 as observed for 750°C calcined sample. These observations clearly signify the role of ceria in preventing the catalyst deactivation and maintaining a high and stable

Table 2

Binding energy value of used $\text{TiO}_2\text{-}\text{ZrO}_2$ (TZ), $\text{CeO}_2\text{/TiO}_2\text{-}\text{ZrO}_2$, $\text{V}_2\text{O}_5\text{/TiO}_2\text{-}\text{ZrO}_2$ and $\text{CeO}_2\text{-}\text{V}_2\text{O}_5\text{/TiO}_2\text{-}\text{ZrO}_2$ samples (after time-on-stream measurements).

Sample	Binding energy (eV)				
	O 1s	$\text{Ce } 3d_{5/2}$	$\text{Zr } 3d_{5/2}$	$\text{Ti } 2p_{3/2}$	$\text{V } 2p_{3/2}$
TZ	529.8	—	182.0	458.5	—
$\text{V}_2\text{O}_5\text{/TZ}$	529.7	—	181.9	458.2	517.1
$\text{CeO}_2\text{/TZ}$	529.8	882.2	181.9	458.5	—
$\text{CeO}_2\text{-}\text{V}_2\text{O}_5\text{/TZ}$	529.8	881.7	182.0	458.3	516.7

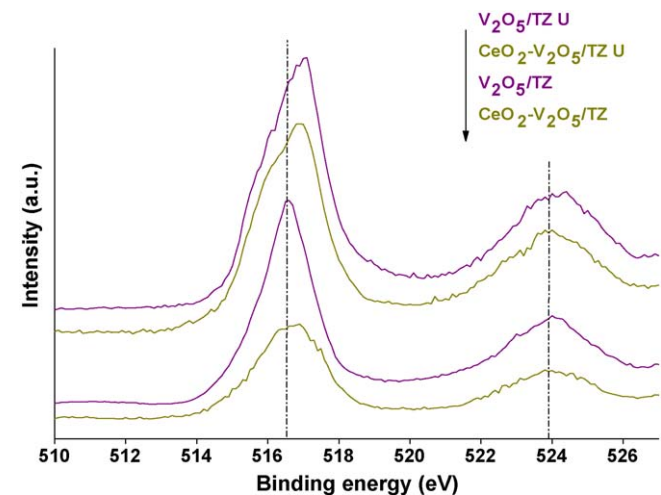


Fig. 11. V 2p core level XPS profiles of fresh and used (U), $\text{V}_2\text{O}_5\text{/TiO}_2\text{-}\text{ZrO}_2$ and $\text{CeO}_2\text{-}\text{V}_2\text{O}_5\text{/TiO}_2\text{-}\text{ZrO}_2$ samples.

activity. Table 2 presents the electron binding energy values of various used samples. As presented in Table 2, the binding energy values of O 1s, Zr 3d, and Ti 2p are similar for used and fresh samples. These results once again support the XRD findings, i.e. there is no specific change in the Zr and Ti composition under reaction conditions. However, V 2p of $\text{V}_2\text{O}_5\text{/TZ}$ shows a decrease in the binding energy value (Table 2) suggesting changes in the chemical environment of vanadium after activity measurements. As depicted in Fig. 11, the used vanadia containing samples show an increase in the intensity as well as broadening of the XPS signals. Moreover, there is a clear shift in the $\text{V } 2p_{3/2}$ by 0.8 eV, which emphasize the formation of ZrV_2O_7 type mixed oxide over the surface under activity measurements. In conclusion, the catalytic activity results from the present study suggest that vanadia and ceria impregnated titania-zirconia mixed oxides exhibit a stable catalytic activity with high conversion and product selectivity in the ODH of EB to styrene with CO_2 as the soft oxidant.

4. Conclusions

In the present investigation, a 1:1 mole ratio $\text{TiO}_2\text{-}\text{ZrO}_2$ mixed oxide support was prepared by a coprecipitation method and various active components namely, ceria, vanadia and ceria-vanadia were deposited by a wet impregnation method. The resulting samples calcined at 550°C exhibited high specific surface areas. In particular, the TZ support exhibited a high surface area of $207 \text{ m}^2/\text{g}$. X-ray diffraction study of 550°C calcined samples revealed an amorphous nature of TZ support. With increase of calcination temperature (750°C), formation of crystalline ZrTiO_4 compound was observed. In case of $\text{V}_2\text{O}_5\text{/TZ}$ and $\text{CeO}_2\text{-}\text{V}_2\text{O}_5\text{/TZ}$ samples, in addition to ZrTiO_4 peaks, few other characteristic lines due to ZrV_2O_7 and CeVO_4 were observed. The XP spectra of V 2p revealed the existence of V^{4+} species at 550°C and V^{4+} species at

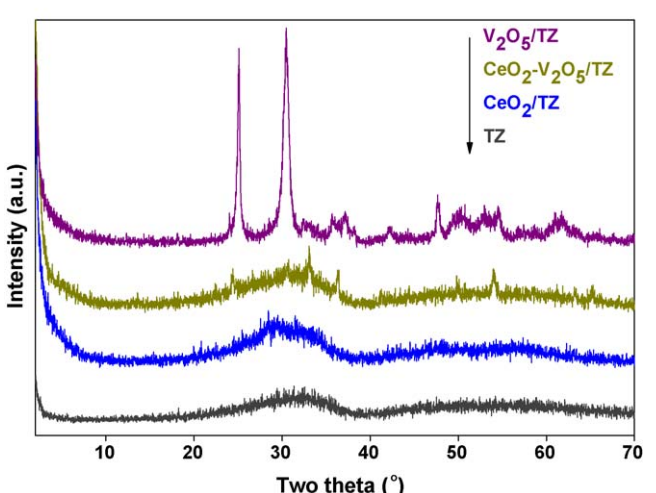


Fig. 10. X-ray powder diffractograms of used $\text{TiO}_2\text{-}\text{ZrO}_2$ (TZ), $\text{CeO}_2\text{/TiO}_2\text{-}\text{ZrO}_2$, $\text{V}_2\text{O}_5\text{/TiO}_2\text{-}\text{ZrO}_2$, and $\text{CeO}_2\text{-}\text{V}_2\text{O}_5\text{/TiO}_2\text{-}\text{ZrO}_2$ samples (after catalytic activity measurements).

750 °C. The XPS profiles of Ce 3d indicated the presence of both Ce⁴⁺ and Ce³⁺ over the TZ support. However, Ti 2p and Zr 3d XPS bands revealed higher oxidation states (4+) for both Zr and Ti. Raman measurements further confirmed the formation of various compounds in the corresponding samples in agreement with XRD results. The TEM analysis suggested the presence of nanosized (<7 nm) particles with narrow range distribution. The TPR studies revealed that the reduction patterns of CeO₂–V₂O₅/TZ sample is a combination of the reduction profiles of CeO₂/TZ and V₂O₅/TZ samples with a low temperature shift suggesting the significant role of ceria addition. Among all the catalysts evaluated, the CeO₂–V₂O₅/TZ combination sample exhibited highest conversion (56%) and product selectivity (98%). Contrarily, the V₂O₅/TZ sample showed a better activity in the first few hours and a faster deactivation was observed with time-on-stream owing to the coke formation. The remarkable ability of CeO₂ in V₂O₅/TZ catalysts to achieve a high and stable activity is clearly apparent from the present study.

Acknowledgements

K. Narayana Rao thanks LNGC, Inha Industry Partnership Institute for inviting as a guest PhD student. This work was financially supported by Saudi Basic Industries Corporation (SABIC) and Korea Federation of Science & Technology (KOSEF).

References

- [1] E.H. Lee, Catal. Rev. Sci. Eng. 8 (1973) 285–305.
- [2] S.-E. Park, J.-S. Chang, K.-W. Lee (Eds.), Stud. Surf. Sci. Catal., vol. 153, Elsevier, Amsterdam, 2004, p. xiii.
- [3] W.D. Mross, Catal. Rev. Sci. Eng. 25 (1983) 591–637.
- [4] N.R. Shiju, M. Anilkumar, S.P. Mirajkar, C.S. Gopinath, B.S. Rao, C.V. Satyanarayana, J. Catal. 230 (2005) 484–492.
- [5] B.M. Reddy, P. Lakshmanan, S. Loridant, Y. Yamada, T. Kobayashi, C.L. Cartes, T.C. Rojas, A. Fernandez, J. Phys. Chem. B 110 (2006) 9140–9147.
- [6] B.A. Banares, Catal. Today 51 (1999) 319–0348.
- [7] C.R. Adams, T.J. Jennings, J. Catal. 17 (1970) 157–177.
- [8] S. Chen, Z.F. Qin, X. Xu, J.G. Wang, Appl. Catal. A: Gen. 302 (2006) 185–192.
- [9] R.M. Freire, F.F. de Sousa, A.L. Pinheiro, E. Longhinotti, J.M. Filho, A.C. Oliveira, P.T.C. Freire, A.P. Ayala, A.C. Oliveira, Appl. Catal. A: Gen. 359 (2009) 165–179.
- [10] A. Sun, Z. Qin, S. Chen, J. Wang, J. Mol. Catal. A: Chem. 210 (2004) 189–195.
- [11] B.S. Liu, R.Z. Chang, L. Jiang, W. Liu, C.T. Au, J. Phys. Chem. C 112 (2009) 15490–15501.
- [12] B.M. Reddy, H. Jin, D.-S. Han, S.-E. Park, Catal. Lett. 124 (2008) 357–363.
- [13] D.R. Burri, K.-M. Choi, S.-C. Han, S.B. Koo, S.-E. Park, Catal. Today 115 (2006) 242–247.
- [14] D.R. Burri, K.-M. Choi, S.-C. Han, A. Burri, S.-E. Park, J. Mol. Catal. A: Chem. 269 (2007) 58–63.
- [15] S. Kaneko, T. Arakawa, M. Ohshima, H. Kurokawa, H. Miura, Appl. Catal. A: Gen. 56 (2009) 80–87.
- [16] B. Xiang, C. Yu, H. Xu, W. Li, Catal. Lett. 125 (2008) 90–96.
- [17] L. Wang, J. Zhang, D.S. Su, Y. Ji, X. Cao, F.F. Xiao, Chem. Mater. 19 (2007) 2894–2897.
- [18] V. Vislovskiy, J. Chang, M. Park, S. Park, Catal. Commun. 3 (2002) 227–231.
- [19] N. Mimura, I. Takahara, M. Saito, T. Hattori, K. Ohkuma, M. Ando, Catal. Today 45 (1998) 61–64.
- [20] B.M. Reddy, D.-S. Han, N. Jiang, S.-E. Park, Catal. Surv. Asia 12 (2008) 1–14.
- [21] B. Murugan, A.V. Ramaswamy, J. Am. Chem. Soc. 129 (2007) 3062–3063.
- [22] B.M. Reddy, A. Khan, Catal. Rev. Sci. Eng. 47 (2005) 257–296.
- [23] B.M. Reddy, K.N. Rao, G.K. Reddy, A. Khan, S.-E. Park, J. Phys. Chem. C 111 (2007) 18751–18758.
- [24] B.M. Reddy, B. Manohar, S. Mehdi, J. Solid State Chem. 97 (1992) 233–238.
- [25] B.M. Reddy, S.-C. Lee, D.-S. Han, S.-E. Park, Appl. Catal. B: Environ. 87 (2009) 230–238.
- [26] B.M. Reddy, P. Bharali, P. Saikia, A. Khan, S. Loridant, M. Muhler, W. Grunert, J. Phys. Chem. C 111 (2007) 10478–10483.
- [27] A. Trovarelli, G. Dolcetti, C. de Leitenburg, J. Kaspar, P. Finetti, A. Santoni, J. Chem. Soc., Faraday Trans. 1 (88) (1992) 1311–1319.
- [28] R.S. Monteiro, L.C. Dieguez, M. Schmal, Catal. Today 65 (2001) 77–79.
- [29] H. Zhang, A. Zhu, X. Wang, Y. Wang, C. Shi, Catal. Commun. 8 (2007) 612–618.
- [30] C.T. Campbell, C.H.F. Peden, Science 309 (2005) 713–714.
- [31] S.T. Oyama, G.T. Went, K.B. Lewis, A.T. Bell, G.A. Somorjai, J. Phys. Chem. 93 (1989) 6786–6790.
- [32] G.C. Bond, S.F. Tahir, Appl. Catal. 71 (1991) 1–7.
- [33] B.M. Reddy, K.N. Rao, G.K. Reddy, P. Bharali, J. Mol. Catal. A: Chem. 253 (2006) 44–51.
- [34] J.A. Mejias, V.M. Jimenez, G. Lassaleta, A. Fernandz, J.P. Espinos, A.R. Gonzalez-Elipe, J. Phys. Chem. 100 (1996) 16255.
- [35] M.-G. Fereres, R. Mariscal, L.J. Alemany, J.L.G. Fierro, J.A. Anderson, J. Chem. Soc., Faraday Trans. 90 (1994) 3711–3718.
- [36] G.A. Sawatzky, D. Post, Phys. Rev. B 20 (1979) 1546–1555.
- [37] P. Victor, S.B. Krupanidhi, J. Phys. D: Appl. Phys. 38 (2005) 41–50.
- [38] A. Burroughs, A. Hammett, A.F. Orchard, G. Thornton, J. Chem. Soc., Dalton Trans. 1 (1976) 1686–1698.
- [39] M. Kilo, C. Schild, A. Wokaun, A. Baiker, J. Chem. Soc., Faraday Trans. 1 88 (1992) 1453–1457.
- [40] M. Andrianainarivelo, R.J.P. Corriu, D. Leclercq, P.H. Mutin, A. Vioux, J. Mater. Chem. 7 (1997) 279–284.
- [41] C.S. Su, A.T. Bell, J. Phys. Chem. B 102 (1998) 7000–7007.
- [42] B.M. Reddy, A. Khan, Y. Yamada, T. Kobayashi, M. Aouine, S. Loridant, J.C. Volta, J. Phys. Chem. B 109 (2005) 3355–3363.
- [43] J.-C. Wu, C.-S. Chung, C.-L. Ay, I. Wang, J. Catal. 87 (1984) 98–107.
- [44] H. Bosch, B.J. Kip, J.G. van Ommeren, P.J. Gellings, J. Chem. Soc., Faraday Trans. 80 (1984) 2479–2488.
- [45] A. Lisovskii, C. Aharoni, Catal. Rev. Sci. Eng. 36 (1994) 25–74.